Journal of Computational Neuroscience 18, 343–352, 2005

Two-Cell to N-Cell Heterogeneous, Inhibitory Networks: Precise Linking of Multistable and Coherent Properties

F.K. SKINNER*
Toronto Western Research Institute, University Health Network, Depts. of Medicine (Neurology), Physiology and Institute of Biomaterials and Biomedical Engineering, University of Toronto, Toronto, Ontario, Canada
fskinner@uhnres.utoronto.ca

H. BAZZAZI AND S.A. CAMPBELL
Department of Applied Mathematics, University of Waterloo, Waterloo, Ontario, Canada

Received December 1, 2004; Revised December 21, 2004; Accepted January 5, 2004

Abstract. Inhibitory networks are now recognized as being the controllers of several brain rhythms. However, experimental work with inhibitory cells is technically difficult not only because of their smaller percentage of the neuronal population, but also because of their diverse properties. As such, inhibitory network models with tight links to the experimental data are needed to understand their contributions to population rhythms. However, mathematical analyses of network models with more than two cells is challenging when the cellular models involve biophysical details. We use bifurcation analyses and simulations to show that two-cell analyses can quantitatively predict N-cell ($N = 20, 50, 100$) network dynamics for heterogeneous, inhibitory networks. Interestingly, multistable states in the two-cell system are manifest as different and distinct coherent network patterns in the N-cell networks for the same parameter sets.

Keywords: basket cell, hippocampus, synchrony, bifurcation analysis, simulations

1. Introduction

Interneurons, or inhibitory GABAergic cells in the hippocampus and cortex represent about 10–20% of the total neuronal population. They express diversity in their biochemical content, morphology, electrophysiological characteristics and neuromodulator sensitivites (McBain and Fisahn, 2001). However, much work on interneurons in recent years is producing well-defined characteristics of interneurons that are functionally significant. In particular, parvalbumin-containing basket cells of hippocampus seem to make up a relatively unmodifiable inhibitory network population responsible for generating gamma (20–80 Hz) and theta (8–12 Hz) rhythms (Freund, 2003). To understand the generation and control of population rhythms such as those generated by basket cells, we need to understand how the various biophysical characteristics contribute to interneuron coherence. One could envisage developing models of individual hippocampal interneurons that encompass the richness of their intrinsic properties. However, this is a non-trivial undertaking and the experimental data is usually lacking in several parameters. Furthermore, many parameters such as those involving the distribution of channel densities are technically difficult to derive. However, if one then uses a simplified model, one must determine how best to constrain the chosen parameters which in turn depend on what the parameters represent.

Heterogeneity of inputs to inhibitory networks strongly affect their ability to synchronize (Golomb

*To whom all correspondence should be addressed.

et al., 2001; Tiesinga and José, 2000; Wang and Buzsáki, 1996; White et al., 1998). This heterogeneity can be thought of as representing an intrinsic neuronal variability and/or a variability in afferent drive. White et al. (1998) considered mildly heterogeneous (<5% difference in intrinsic frequencies) two-cell networks and identified two different ways in which coherence could be lost. This occurred in two different regimes, termed phasic and tonic, as identified by different values of the ratio of time constant and network period. Their work shed light on why optimal synchronization at particular frequencies might be obtained in the larger networks examined in the same paper and also in Wang and Buzsáki (1996). That is, their two-cell network studies helped understand the qualitative states of N-cell circuits with $N \gg 2$.

In recent work (Skinner et al., 2004) we examined the changing dynamics of two-cell inhibitory networks in which the amount of input heterogeneity was varied. We found that an optimal set of parameters could be obtained for the given cellular model (with its various biophysical characteristics) based on the ability of the two-cell network to synchronize in the face of heterogeneity. In particular, for the Wang-Buzsáki model, we found that near-synchronous behaviour occurred for a >11% difference in intrinsic frequencies of the two cells for specific parameter sets that are within experimentally determined values. In addition, we found that the two-cell coherence properties and bistable outputs were maintained in ten-cell networks for the same parameter sets. Given that White and colleagues found a qualitative correspondence in dynamics from two- to ten- and 100-cell networks, this is not completely surprising. However, it is far from clear whether there should be any precise and quantitative correspondences between two-cell and $N(\gg 2)$-cell network dynamics. Such quantification would be helpful in making tighter links with biophysical, experimental data. In this paper, we perform focused and detailed explorations with specific parameter sets using bifurcation analyses of two-cell networks, and simulations of 20, 50 and 100-cell networks. We find that the two-cell analyses predict the dynamics of the larger network simulations quite precisely.

2. Model and Methods

We use a single compartment model developed by Wang and Buzsáki (WB) (1996) to represent the intrinsic properties of a hippocampal interneuron cell. The equations for each cell are given by:

$$C\frac{dV}{dt} = I_{\text{app}} - g_{\text{Na}}m_\infty^3 h(V - V_{\text{Na}}) - g_{\text{K}}n^4(V - V_{\text{K}}) - g_L(V - V_L) \quad (1)$$

$$\frac{dh}{dt} = \phi(\alpha_h(V)(1 - h) - \beta_h(V)_h) \quad (2)$$

$$\frac{dn}{dt} = \phi(\alpha_n(V)(1 - n) - \beta_n(V)n) \quad (3)$$

where V is the cell membrane voltage in mV, h is the inactivation of the sodium current, n is the activation of the potassium current, and t is time in ms. m_∞ is the steady state activation of the sodium current and is given by: $m_\infty = a_m/(a_m + \beta_m)$, where $a_m(V) = -0.1(V + 35)/(\exp(-0.1(V + 35)) - 1)$, $\beta_m(V) = 4\exp(-(V + 60)/18)$. $a_h(V) = 0.07\exp(-(V + 58)/20)$, $\beta_h(V) = 1/(\exp(-0.1(V + 28)) + 1)$, $\alpha_n(V) = -0.01\exp(-(V+34)/\exp(-0.1(V+34))-1)$, $\beta_n(V) = 0.125\exp(-(V + 44)/80)$, $\phi = 5$. Maximal sodium, g_{Na}, potassium, g_{K}, and leak, g_L, conductances are: 35, 9 and 0.1 mS/cm^2 respectively. Reversal potentials, V_{Na}, V_{K}, V_L, are 55, −90 and −65 mV respectively, and the capacitance, C, is 1 μF/cm^2.

We consider neuronal networks formed due to coupling via inhibitory synapses that are described by first order kinetics. The inhibitory synaptic current, I_{syn}, which would be added to the current balance equation of the postsynaptic cell, is given by:

$$I_{\text{syn}} = g_{\text{syn}}s(V - V_{\text{syn}}) \quad (4)$$

where

$$\frac{ds}{dt} = \alpha T(V_{\text{pre}})(1 - s) - s/\tau_{\text{syn}} \quad (5)$$

$$T(V_{\text{pre}}) = \frac{1}{1 + \exp(-V_{\text{pre}}/2)} \quad (6)$$

and V_{pre} is the voltage of the presynaptic cell, g_{syn} is the maximal inhibitory synaptic conductance, $V_{\text{syn}} = -75$ mV is the synaptic reversal potential, $\alpha = 6.25\ \text{ms}^{-1}$ is the rate constant of the synaptic activation taken from Bartos et al. (2001), and τ_{syn} is the synaptic decay time constant. τ_{syn} values as low as 1 ms were measured between hippocampal basket cells (Bartos et al., 2002), and so we explore a τ_{syn} range of 1 to 10 ms in our simulations, with a 1 ms resolution. For the purposes of this paper, we focus on a g_{syn} value of 0.25 mS/cm^2, which is within experimentally determined values (Bartos et al.,

2001, 2002). Additional values have been considered in our previous work (Skinner et al., 2004).

I_{app} represents the applied or external drive to the cell, and we use this parameter to introduce heterogeneity into the system. We consider two-cell networks that are reciprocally coupled and 20, 50 and 100-cell all-to-all coupled networks.

For the two-cell networks, the external drive to cell 1 or 2 is:

$$I_{\text{app},1} = I_\mu - \epsilon \quad \text{or}$$
$$I_{\text{app},2} = I_\mu + \epsilon$$

respectively, so that their external drives differ by 2ϵ. We define the percent heterogeneity, %Het, as:

$$\%\text{Het} = \frac{(I.F.\text{ at } I_{\text{app},2}) - (I.F.\text{ at } I_{\text{app},1})}{I.F.\text{ at } I_{\text{app},2}} \times 100\% \tag{7}$$

where $I.F.$ is the intrinsic frequency of the isolated cell. I_μ values of 1 and 3 μA/cm^2 are explored. We fit a 4th order polynomial to the $I.F.$ versus I_{app} curve to allow consistent calculation of %Het values. The equation describing this fit is given by:

$$I.F.(I_{\text{app}}) = -0.112I_{\text{app}}^4 + 1.88I_{\text{app}}^3 - 13.1I_{\text{app}}^2 + 70.5I_{\text{app}} + 0.258 \tag{8}$$

where $I.F.$ is in units of Hz and I_{app} is in units of μA/cm^2. This is illustrated in Fig. 1. We perform bifurcation analyses and numerical continuations of the two-cell networks using AUTO (Doedel, 1981) in the XPPAUT software package (Ermentrout, 2002).

For the 20, 50 and 100-cell networks, the I_{app}'s are randomly chosen in the interval [$-$%Het, $+$%Het]. In the all-to-all coupled network simulations, g_{syn} values are normalized so that each presynaptic cell "delivers" a maximal inhibition of $g_{\text{syn}}/(N-1)$. We perform network simulations using our in-house software, NNET, which is described in Murray (2004) and Skinner and Liu (2003). Integration of the system of differential equations is done using either CVODE or Runge-Kutta methods, and using a tolerance of 10^{-6} or less and a stepsize of .01 ms. We consider two different types of intial conditions (ICs) which can be thought of as "hyperpolarized" or "depolarized" conditions. Hyperpolarized conditions: $V_i = -100.0 + [0.0, 50.0]$, $h_i = 0.99$, $n_i = 0.01$, $s_i = 0.01$; depolarized conditions: $V_i = -50.0 + [0.0, 50.0]$, $h_i = 0.01$, $n_i = 0.99$, $s_i = 0.99$. The square brackets indicate the interval from which a value is randomly obtained. At least 5, 10 and 20 different sets of ICs are used for the 100, 50 and 20-cell network simulations respectively, and for several different %Het values, resulting in excess of 3000 sets of simulations. Although the choice of these numbers is somewhat arbitrary, they were enough to show the 2-cell to N-cell linkage features of this paper. We use a coherence measure based on White et al. (1998). This measure is essentially a cross correlation that approximates the amount of overlap that exists between two spiking cells where the amount of overlap used is 20% of the period of the faster firing cell. The average between all pairs is calculated to give a mean coherence measure. In addition, we visually inspect several raster plots to gauge the mean coherence measures. This is necessarily a subjective measure but the combined analysis of the coherence measure and visual inspection of raster plots is enough to chracterize the non-monotonic and multistable features described in this work. Units for g_{syn}, τ_{syn} and I_μ are always given in mS/cm^2, ms and μA/cm^2 respectively.

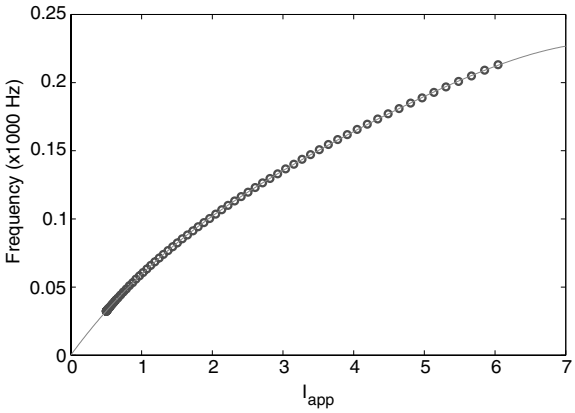

Figure 1. Frequency versus I_{app} for the Isolated Cell. Circles represent data points determined using AUTO for an individual model neuron, and the curve is a 4th order polynomial fit given by Eq. (8) in Methods. I_{app} is in units of μA/cm^2.

3. Results

We know from previous work that several distinct patterns can be produced by two-cell, heterogenous inhibitory networks (Skinner et al., 2004; White et al., 1998). These patterned states involve phase-locked states (near-synchronous and near-antiphase), suppressed states, harmonic locking, and asynchronous

states. In general, one must turn to numerical simulations to investigate the dynamics of $N(\gg 2)$-cell networks of spiking neurons, as analytical work becomes prohibitive. As such, it would be helpful if one could translate two-cell network analyses to an understanding of dynamic mechanisms underlying N-cell network output. To consider how two-cell dynamics might be linked to N-cell dynamics, we take the following view: If one randomly distributes inputs to N cells of an N-cell inhibitory (all-to-all coupled) network in a range up to a maximal amount of heterogeneity, say $\%\text{Het}_{\max}$, then the possible patterns that the N-cell networks express include the particular patterns that the two-cell inhibitory networks express with $\%\text{Het} \leq \%\text{Het}_{\max}$. It is not obvious that this view we propose should be the case for heterogeneous networks, as additional dynamics could emerge in the larger networks to nullify the effects of the specific dynamics observed in the two-cell networks. To examine this view, we focus on two of our previous observations (Skinner et al., 2004). First, there is a non-monotonic dependence of robustness of network oscillations on τ_{syn}, where robustness is given by the maximal %Het for which the two-cell network expresses near-synchronous behaviour. Second, multistable patterns in two-cell networks occur in larger networks for the same parameter values. In this paper, we focus on a fixed maximal synaptic conductance value, but explore a range of τ_{syn} values ($1 - 10$ ms) and two different I_μ values. These values not only encompass the richness of the dynamics, but also constitute physiologically reasonable network frequencies, and g_{syn} and τ_{syn} values are within experimentally determined values (Bartos et al., 2001, 2002).

3.1. Two-Cell Bifurcation Analyses

We first describe the results of bifurcation analyses and numerical continuations of the two-cell heterogeneous networks. We followed three different types of oscillatory solutions: near-synchronous solutions, near-antiphase solutions and suppressed state solutions (either cell 1 suppressing cell 2 or vice versa). In Fig. 2A, we show an example bifurcation diagram with I_μ as the bifurcation parameter. One can see that unstable suppression oscillations emanate from two Hopf bifurcations whereas stable ones are created via saddle node of limit cycle bifurcations. Near-synchronous oscillations are also created via saddle node of limit cycle bifurcations.

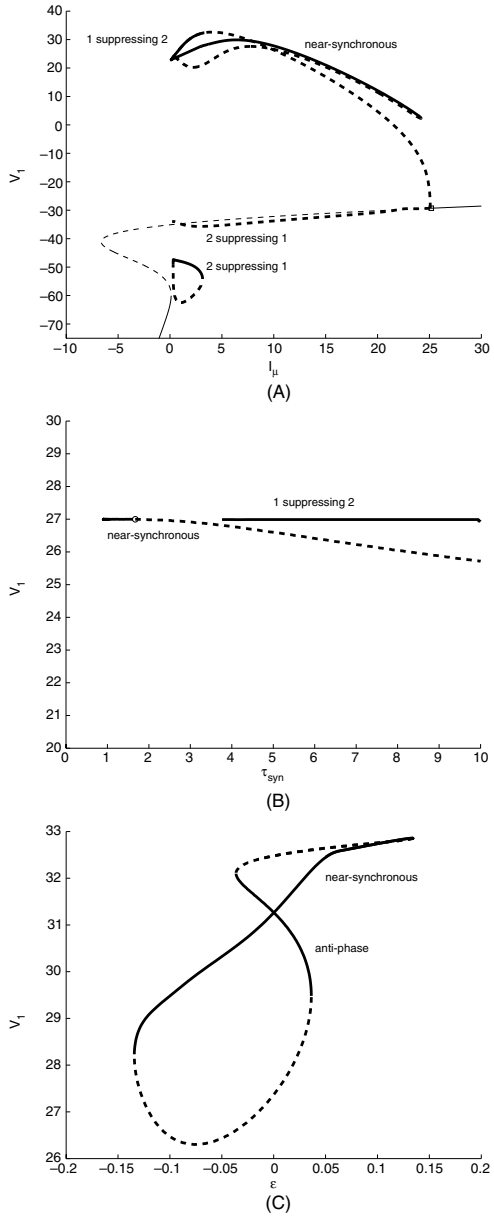

Figure 2. Example Bifurcation Diagrams. Each diagram shows the maximum value of V_1 (in mV) for each value of the bifurcation parameter. Stable/unstable equilibria are denoted by thin solid/dashed lines; stable/unstable periodic solutions by thick solid/dashed lines. Hopf bifurcations are indicated by an open box, period doubling by an open circle. (A) I_μ (in μA/cm^2) is the bifurcation parameter; other parameters are $g_{\text{syn}} = 0.25$ mS/cm^2, $\epsilon = 0.05$ μA/cm^2, Note the region of multistability between near-synchronous and both suppression oscillations. $\tau_{\text{syn}} = 10$ ms. (B) τ_{syn} (in ms) is the bifurcation parameter; other parameters are $g_{\text{syn}} = 0.25$ mS/cm^2, $\epsilon = 0.05$ μA/cm^2, $I_\mu = 1$ μA/cm^2 (C) ϵ (in μA/cm^2) is the bifurcation parameter; other parameters are $g_{\text{syn}} = 0.25$ mS/cm^2, I_μ, $= 3$ μA/cm^2, $\tau_{\text{syn}} = 1$ ms. Note the region of multistability between the near-synchronous and anti-phase oscillations.

By performing continuations using τ_{syn} and ϵ as the bifurcation parameter, we were able to determine %Het bounds for which these different solutions occurred stably. Example bifurcation diagrams with τ_{syn} and ϵ as the bifurcation parameter are shown in Fig. 2B and 2C respectively. From continuations performed in AUTO, we obtain ϵ bounds for stable near-synchronous (Table 1), near-antiphase (Table 2) and suppressed (Table 3) solutions. In particular, note the non-monotonic relationship between the maximal ϵ and τ_{syn} as shown in Table 1. τ_{syn} values between 4.25 and 5.75 produce

Table 1. ϵ Bifurcation parameter results for near-synchronous solutions.

Parameters (I_μ, τ_{syn})	Max ϵ	%Het
(3,1)	0.134	5.87
(3,2)	0.190	8.23
(3,3)	0.231	9.92
(3,4)	0.254	10.86
(3,4.25)	0.258	11.02
(3,5)	0.267	11.38
(3,5.75)	0.273	11.63
(3,6)	0.218	9.39
(3,7)	0.184	7.98
(3,8)	0.164	7.14
(3,9)	0.149	6.51
(3,10)	0.136	5.95
(1,1)	0.0533	8.5
(1,1.5)	0.0706	11.12
(1,8)	0.0136	2.24
(1,9)	0.0134	2.21
(1,10)	0.0128	2.1

Table 2. ϵ Bifurcation parameter results for near-antiphase solutions.

Parameters (I_μ, τ_{syn})	Max ϵ	%Het
(3,1)	0.0363	1.62
(3,1.1)	0.0287	1.29
(3,1.2)	0.0214	0.96
(1,1)	0.0264	4.3
(1,1.2)	0.0237	3.87
(1,1.4)	0.0199	3.26
(1,1.6)	0.0152	1.90
(1,2)	0.0052	0.86

Table 3. ϵ Bifurcation parameter results for suppressed solutions.

Parameters ($I_\mu \tau_{\text{syn}}$)	Min ϵ (1 suppressing 2)	%Het	Max ϵ (2 suppressing 1)	%Het
(3,1)	2.04	69.97	<0	<0
(3,2)	1.48	53.04	<0	<0
(3,3)	1.07	40.14	<0	<0
(3,4)	0.775	30.28	<0	<0
(3,5)	0.543	22.01	<0	<0
(3,6)	0.358	15.00	<0	<0
(3,7)	0.205	8.85	<0	<0
(3,8)	0.0773	3.43	<0	<0
(3,9)	<0	<0	0.0321	1.44
(3,10)	<0	<0	0.0127	0.57
(1,1)	0.515	61.93	<0	<0
(1,2)	0.307	41.24	<0	<0
(1,3)	0.147	21.88	<0	<0
(1,4)	0.0234	3.82	<0	<0
(1,5)	<0	<0	0.074	11.56
(1,6)	<0	<0	0.151	22.42
(1,7)	<0	<0	0.215	30.57
(1,8)	<0	<0	0.268	36.85
(1,9)	<0	<0	0.313	41.89
(1,10)	<0	<0	0.351	45.97

Max%Het in excess of 11%. For the antiphase solutions, it was not possible to perform continuations for some of the τ_{syn} values. For these cases, a phase reduction model was investigated (not shown). It indicated that antiphase solutions are stable for $\tau_{syn} = 1, 2$ when $I_\mu = 1$, but only for $\tau_{\text{syn}} = 1$ when $I_\mu = 3$. The phase reduction model also indicated the presence of stable near-synchronous solutions for $\tau_{syn} = 1 - 10$ for both $I_\mu = 1$ and 3. This is consistent with our bifurcation analysis for $I_\mu = 3$. For $I_\mu = 1$ we were not able to continue the near-synchronous solutions for all values of τ_{syn}. This was due to a loss of stability of these solutions through a period doubling bifurcation, resulting in a very small range of %Het values where they were stable. This was supported by continuations using τ_{syn} as the bifurcation parameter (see Fig. 2B). For the suppressed solutions, there are two to consider (see Fig. 2A). Results shown in Table 3 indicate the ϵ bounds; the upper bound (max ϵ) is for the solution in which cell 2 suppresses cell 1, and the lower bound is for the solution in which cell 1 suppresses cell 2. Clearly, if the min ϵ bound is negative, suppressed solutions are present for all %Het values.

From these results, we can easily see where multistability occurs. For example, bistability between (near) synchronous and antiphase solutions occurs for $\tau_{\text{syn}} = 1$ up to 4.3%Het when $I_\mu = 1$, but only up to 1.6%Het when $I_\mu = 3$. Also, bistability between near-synchronous and suppression solutions exist for all $\tau_{\text{syn}} > 8$ when $I_\mu = 1$ or 3. Armed with these results, we now examine N-cell network simulations to see whether and how our view of two-cell to N-cell dynamics might be manifest.

3.2. N(≫2)-Cell Simulations

Let us first focus on a parameter set that only exhibits the near-synchronous solution (of the different solutions followed) in the two-cell heterogeneous network system. For $\tau_{\text{syn}} = 6$, $I_\mu = 3$, the two-cell system expresses stable, near-synchronous oscillations up to 9.39%Het, and stable near-antiphase and suppressed state solutions do not exist for these parameter values. Figure 3 shows 20, 50 and 100-cell raster plots for these τ_{syn} and I_μ parameter values and 8%Het. Since this %Het is within the %Het value obtained from the two-cell analyses, based on our view above, we would predict the existence of coherent network states since stable near-synchronous solutions are present up to 9.39%. In Fig. 3, we see that coherence clearly exists in the N-cell networks for these parameters, and this was the case for 35 different sets of initial conditions used. Therefore, the simple view described above appears useful in the quantification we seek.

Next, we examined the network behaviour as the %Het was increased. In Fig. 4, we plot the mean coherence measure from 50-cell networks versus ϵ (equivalent to %Het) for seven different %Het values with $\tau_{\text{syn}} = 3$ or 5, and $I_\mu = 3$. For these parameter values, we know from the two-cell network analyses, that near-synchronous solutions exist up to approximately 10%Het and 11.4%Het for $\tau_{\text{syn}} = 3$ and 5 respectively. From Fig. 4, it is clear that as %Het increases, coherence decreases. This is not too surprising given that as %Het increases, the spikes become less neatly lined up to produce their coherent patterns, leading to a decreased mean coherence value. This decreasing coherence with increasing %Het was also true for the 20-cell and 100-cell networks. Visual inspection of several raster plots with parameters as in Fig. 4 indicates that any coherence is difficult to see beyond 11.4%Het. Although subjective, this is suggestive of the notion that the maximal ϵ values obtained from the two-cell analyses is an indicator of the limits of possible heterogeneity that support coherent behaviours in large networks.

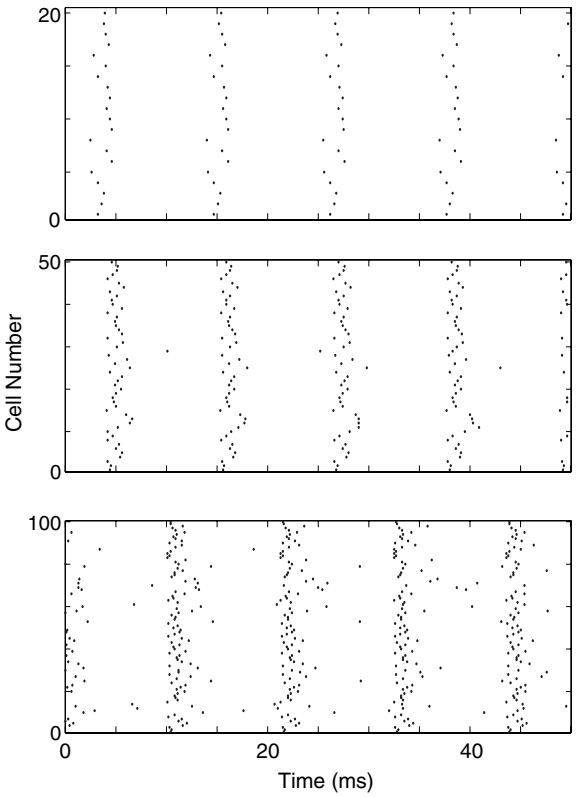

Figure 3. Coherence in N-cell Networks. Raster plots from 20-cell, 50-cell and 100-cell network simulations. The x-axis shows time in ms and the y-axis is the cell number. Each dot represents the time where a spike is produced by the particular cell. $I_\mu = 3\ \mu\text{A/cm}^2$, $\tau_{\text{syn}} = 6$ ms, and 8%Het. Coherent patterns are visually unambiguous. Calculated mean coherence values for these example raster plots are 0.54 (100-cell), 0.63 (50-cell) and 0.68 (20-cell).

Now let us focus on the first of our previous observations: there is a non-monotonic dependence of the maximal %Het on τ_{syn}. Since we observed (above) that the maximal ϵ values obtained from two-cell analyses indicate heterogeneity limits of coherent behaviour in large networks, we examined the mean coherence values in our networks for various %Het values, reasoning that the non-monotonic relationship could be reflected in this way if it were present. We find that the two-cell non-monotonic observation is preserved in mean coherence versus τ_{syn} relationships for 20, 50 or 100-cell network simulations. We illustrate this in Fig. 5 for the 50-cell simulations and 9.0%Het. Figure 5 shows a plot of mean coherence values versus τ_{syn} for two different sets of initial conditions, as well as an

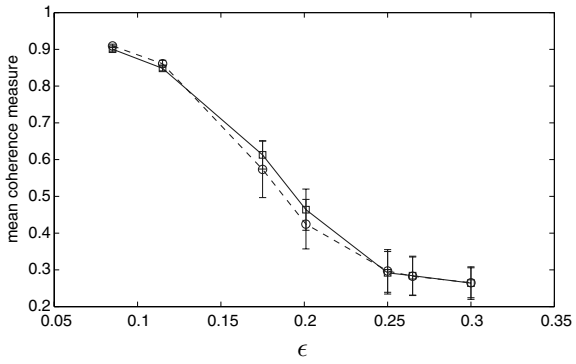

Figure 4. Increasing Heterogeneity Decreases Coherence. Plot of the mean coherence measure versus ϵ (in μA/cm^2) for $\tau_{syn} = 3$ and 5 ms, for 7 different %Het values. Each point is the average mean coherence measure from simulations with 10 different initial conditions, and the error bars are $\pm$ standard deviation. Circles joined with dashed lines refer to $\tau_{syn} = 3$, and squares joined with solid lines refer to $\tau_{syn} = 5$. The ϵ values correspond to %Het values of 3.8%, 5.2%, 7.7%, 9.0%, 10.8%, 11.4% and 12.9%. Calculations are for 50-cell networks, $I_\mu = 3$ μA/cm^2.

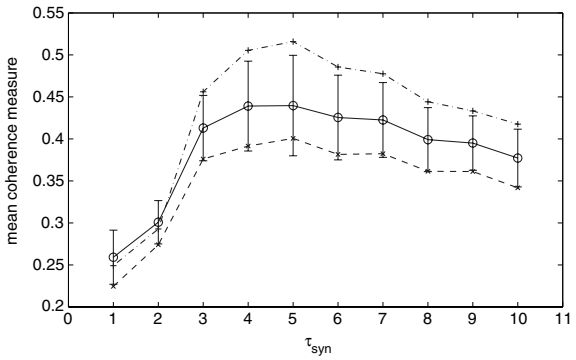

Figure 5. Non-monotonic Coherence Dependence On τ_{syn}. Plot of the mean coherence measure versus τ_{syn} (in ms) for 50-cell networks, $I_\mu = 3$ μA/cm^2 and 9.0%Het. Open circles joined by solid lines are the average mean coherence measure from simulations with 6 different sets of initial conditions (ICs) and the error bars are $\pm$ standard deviation. Dashed and dashed-dotted lines joining x's and +'s respectively represent mean coherence measure values from 2 particular sets of ICs.

average, all showing a non-monotonic relationship. It is important to note that the actual value for the mean coherence by itself is not a sufficient characterization of the network dynamics. That is, it is biased by the bin size (we use 20% overlap of the faster firing cell), network size being examined, particular network dynamics being expressed (e.g., bursting, spike-to-spike synchrony, clustering), and so on. In particular, because of the increase in network period with increasing τ_{syn} (not shown), the coherence measure could be biased upwards for larger τ_{syn} values. Moreover, the presence of multistable patterning (see Tables 1–3) could also bias these measures. Better measures could be developed for particular investigations, but for the work here, we find that visual examination of the raster plots together with the simple correlation measure (i.e., mean coherence value) is enough to determine whether and how two-cell to N-cell linkages might occur. Therefore, although the error bars are large, it was clear that any set of network simulations (20, 50 or 100 cells) gave rise to a non-monotonic relationship for any particular random set of initial conditions, and for different %Het's.

Our second area of focus is on multistable patterns. Consider three distinct cases. In the first case, consider $I_\mu = 1$, $\tau_{syn} = 1$, and 8%Het. Based on the two-cell analyses, near-synchronous and near-antiphase solutions bistably occur for %Het < 4.3%. Therefore, using 8%Het in N-cell simulations, our view expressed at the beginning of the results would lead us to expect that we might be able to obtain coherent patterns with network frequencies that differ in frequency by two (one network frequency being due to the near-synchronous states, and the other being due to the near-antiphase states). Figure 6A shows raster plots for three different sets of initial conditions, and we see that this is the case. The top raster plot has coherent patterns that have a network period that is about double the period of the middle raster plot. We also obtain network dynamics with no obvious visual coherence, i.e., the bottom raster plot shown in Fig. 6A. At this level of %Het, i.e., 8%Het, and given the multistable patterns that can exist, it is not surprising that non-coherent states also occur in the larger networks. Of ten different initial condition sets used, two produced coherent network patterns that were influenced by near-synchronous states, three produced coherent network patterns that were influenced by near-antiphase states and five produced patterns with no obvious visual coherence. However, if the %Het is made small enough, non-coherent states would no longer be present (see above and Fig. 4). Using 4.8%Het and ten different initial condition sets in N-cell simulations, we obtained six that were influenced by near-synchronous states, three that were influenced by near-antiphase states and only one with no obvious coherence. For the second distinct case, consider $I_\mu = 3$, $\tau_{syn} = 1$, and 3%Het. Based on the two-cell analyses, near-synchronous and near-antiphase

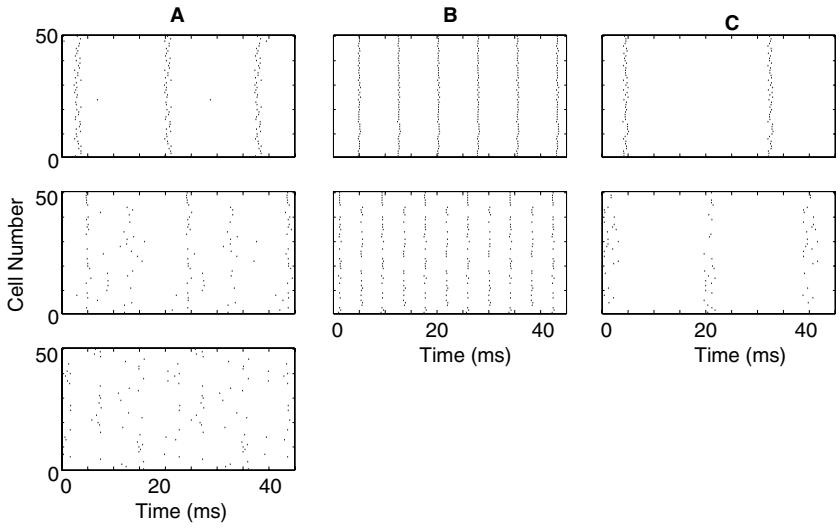

Figure 6. Bistable N-cell Network Patterns. Raster plots from 50-cell network simulations are shown for: (A) $I_\mu = 1$ μA/cm^2, $\tau_{\rm syn} = 1$ ms, and 8.0%Het; (B) $I_\mu = 3$ μA/cm^2, $\tau_{\rm syn} = 1$ ms, and 3.2%Het; (C) $I_\mu = 1$ μA/cm^2, $\tau_{syn} = 7$ ms, and 4.0%Het. Three raster plots are shown for (A) to illustrate the different patterns obtained for different initial conditions (ICs). They can be seen to be influenced by near-synchronous (top raster) and near-antiphase (middle raster) solutions present in the two-cell analyses. We also obtain patterns with no visual coherence (bottom raster). Two raster plots are shown for (B) reflecting near-synchronous (top) and near-antiphase (middle) solutions. Two raster plots are shown for (C). The network patterns can be seen to be influenced by bistable near-synchronous (top) and suppressed (middle) solutions present in the two-cell analyses. Mean coherence values are 0.83 (top), 0.32 (middle), 0.26 (bottom) for (A); 0.93 (top) and 0.46 (middle) for (B); 0.94 (top) and 0.43 (middle) for (C).

solutions are bistable for %Het < 1.6%. As for the first case, network patterns that are clearly influenced by near-synchronous and near-antiphase states are present to give rise to very different network frequencies depending on the initial conditions. This is illustrated in Fig. 6B.

The third distinct case regarding multistability that we illustrate is with $I_\mu = 1$, $\tau_{\rm syn} = 7$, and 4%Het. Based on the two-cell analyses, it is clear that beyond $\tau_{\rm syn} = 4$, there are bistable near-synchronous and suppressed state solutions. Large network simulations that are influenced by suppressed state solutions would be expected to have network periods that are less than those that are influenced by the near-synchronous states, but not as small as half the period, as would be the case if the coherent network patterns were influenced by near-antiphase states (e.g., see Fig. 6A and B). Indeed, network patterns that are influenced by the suppressed states would be expected to have periods that are close to the periods of the isolated cells. In Fig. 6C, we show raster plots for two different sets of initial conditions that show this to be the case. Such bistable network patterns were present for all other $\tau_{\rm syn}$ values where bistable suppressed and near-synchronous solutions occurred, as indicated by the two-cell analyses (see Tables 1 and 3). These multistable patterns were also present in other N($\neq$50)-cell networks. There was no obvious difference in the ability to see multistable patterns and N in our simulations.

Finally, we show that it is possible to separate by different initial conditions, the different networks patterns that arise in the N-cell networks. For this, we focus on $I_\mu = 1$, $\tau_{\rm syn} = 1$, and choose 4%Het which encompasses stable solutions of both near-synchronous and near-antiphase solutions. Given that the heterogeneous inputs for the N-cell network simulations are randomly chosen from a uniform distribution, the choice of 4%Het means that there is not any large bias toward near-synchronous or near-antiphase solutions, as antiphase solutions are stable up to 4.3%Het. For these parameters, all initial conditions from the "hyperpolarized" conditions gave rise to coherent network patterns that were influenced by the near-antiphase states, and all initial conditions from the "depolarized" conditions gave rise to coherent network patterns that were influenced by the near-synchronous states. Some of the raster plots are shown in Fig. 7. Physiologically, this is interesting as it suggests that depending on the "history" of inputs to the inhibitory network (i.e., putting it in a "depolarized" or "hyperpolarized"

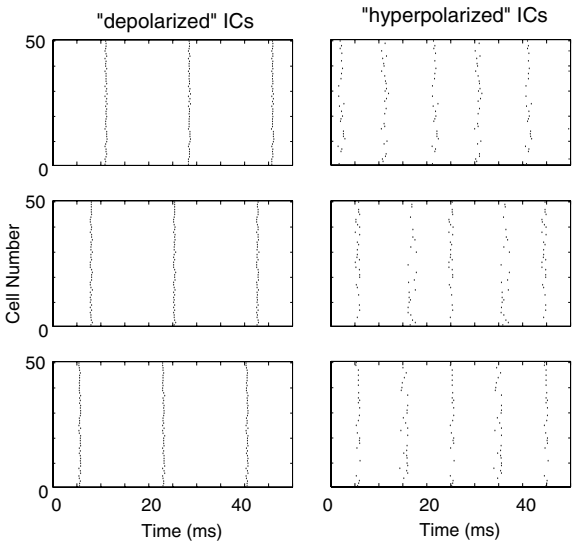

Figure 7. Separation Of Bistable Patterns By Initial Conditions. Raster plots of 50-cell network simulations showing two distinct coherent patterns (as influenced by near-antiphase and near-synchronous bistable states). $I_\mu = 1$ μA/cm^2, $\tau_{syn} = 1$, and 4.0%Het. On the right are raster plots when three different "hyperpolarized" initial conditions (ICs) are used. On the left are raster plots when three different "depolarized" initial conditions (ICs) are used. Mean coherence values are 0.44, 0.43 and 0.44 (top to bottom) for the right raster plots and 0.96 for all three raster plots on the left side.

state), it can be biased to produce network patterns that have drastically different network frequencies. If we increase the %Het to 5%Het so that there is now a potential bias toward near-synchronous solutions based on the two-cell analyses, we still get the different types of network output (see Fig. 6A), but now the separation of network patterns between "depolarized" and "hyperpolarized" initial conditions is no longer there and there are more network patterns that are influenced by the near-synchronous state. Specifically, of five "hyperpolarized" initial conditions, one of them produces a network output that is influenced by the near-synchronous state, and one of them produces no visual coherence (see Fig. 6A). This indicates the preciseness of the N-cell network patterns produced based on the two-cell analyses.

The multistable network patterns observed in the N-cell networks are clearly influenced by near-synchronous, near-antiphase and suppressed states. This influence is made stronger by inspection of network periods. For example, the network period is about 27 ms in Fig. 6C (top) which presumably reflects near-synchronous solutions, whereas it is somewhat less than 20 ms in Fig. 6C (middle), which presumably reflects suppressed state solutions. Given that synchronized output from inhibitory networks have larger periods compared to the individual cell's intrinsic period, and that the isolated cells' periods are 16.5 and 17.2 ms (using Eq. (8) in Methods) for these particular parameters, the linkage is clear. Similar calculations for other bistable patterns also support this observed influence.

4. Discussion

The motivation for this work is to determine how best to make quantitative links with the experimental data. The challenges involved in experimental work involving interneurons with diverse properties demands that tight quantitative links with the experimental data be made. It is clear that detailed, biophysical differences exist, but understanding the importance of these details requires a context. Using the context of interneuron coherence is reasonable given their clear participation in *in vivo* rhythms (Klausberger et al., 2003). Quantifying the difference of the details in various cellular models is needed to understand particular contributions even though qualitative similarities may exist between different models. The results of this work show that quantitative linkages occur between two-cell and N-cell network dynamics since coherent patterns in the N-cell networks can be seen to be due to distinct two-cell patterns for the same parameter sets. As such, the two-cell analyses can be viewed as a quantitative predictor of N-cell dynamics for heterogeneous, inhibitory networks. In particular, (i) non-monotonic coherent relationships versus τ_{syn} are maintained in the larger networks for the same parameter sets, and (ii) multistable patterns in the two-cell system are manifest as different and distinct coherent network patterns in the larger networks for the same parameter sets. Specifically, coherent network patterns with two-fold different frequencies in the N-cell networks occur as a result of near-synchronous and near-antiphase bistable solutions in the two-cell system.

The N-cell networks we model are all-to-all coupled. The value of N that should be used in these investigations is unclear, but it is clearly an additional, important consideration. Golomb et al. (2001) used phase reduction techniques and simulations to show that for massively connected networks, inhibitory networks are more advantageous than excitatory ones in the production of neuronal synchrony. In addition, they considered network architecture in the form of sparse networks.

The use of 20, 50 and 100 cells in our network simulations here seems reasonable since such sizes have been used by several other investigators to understand inhibitory network phenomena (Bartos et al., 2001; Tiesinga and José, 2000; Wang and Buzsáki, 1996, White et al., 1998). Besides network architecture, there are several additional challenges to consider, such as dendritic effects, electrical coupling by gap junctions and appropriate synaptic background activities. Given that one can determine the tissue size (i.e., number of cells) needed to produce spontaneous population oscillations dependent on interneuron coherence (Wu et al., 2004), it will be interesting to investigate the effects of N. Doing simulations with thousands of cells, so as to approach biological numbers will be compelling to perform if one could have some insight on critical biophysical parameters and potential mechanisms from two-cell analyses and experimental observations. It will also be critical to develop more appropriate coherence measures to analyze the network dynamics.

Acknowledgments

This work was supported by NSERC of Canada. F.K.S thanks P. Murray for help with NNET and associated scripts and RIS for computing support.

References

Bartos M, Vida I, Frotscher M, Geiger JRP, Jonas P (2001) Rapid signaling at inhibitory synapses in a dentate gyrus interneuron network. J. Neurosci. 21: 2687–2698.

Bartos M, Vida I, Frotscher M, Meyer A, Monyer H, Geiger JRP, Jonas P (2002) Fast synaptic inhibition promotes synchronized gamma oscillations in hippocampal interneuron networks. Proc. Natl. Acad. Sci., 99(20): 13222–13227.

Doedel EJ (1981) AUTO: A program for the automatic bifurcation analysis of autonomous systems. Congr. Numer., 30: 265–284.

Ermentrout GB (2002) Simulating, Analyzing, and Animating Dynamical Systems: A Guide to XPPAUT for Researchers and Students. SIAM, Philadelphia, http://www.math.pitt.edu/~bard/xpp/xpp.html.

Freund TF (2003) Interneuron diversity series: Rhythm and mood in perisomatic inhibition. Trends Neurosci. 26(9): 489–495.

Golomb D, Hansel D, Mato G (2001) Mechanisms of synchrony of neural activity in large networks. In: S. Gielen, M. Moss, eds., Handbook of Biological Physics, Vol. 4, Elsevier Science B.V., Amsterdam, pp. 887–968.

Klausberger T, Magill P, Márton M, Roberts J, Cobden P, Buzsáki G, Somogyi P (2003). Brain-state- and cell-type-specific firing of hippocampal interneurons *in vivo*. Nature 421: 844–848.

Lewis TJ, Rinzel J (2003). Dynamics of spiking neurons connected by both inhibitory and electrical coupling. J. Comput. Neurosci. 14(3): 283–309.

McBain C, Fisahn A (2001). Interneurons unbound. Nature Rev. Neurosci. 2: 11–23.

Murray PA (2004) Capturing details of short-term synaptic plasticity in simple schemes. Master's Thesis, University of Toronto.

Skinner FK, Chung JYJ, Ncube I, Murray PA, Campbell SA (2004). Using heterogeneity to predict inhibitory network model characteristics. J. Neurophysiol. (in press).

Skinner FK and Liu JB (2003). NNET: Linking small and large-scale network models. Neurocomputing 52–54: 381–387.

Tiesinga PHE, José JV (2000). Robust gamma oscillations in networks of inhibitory hippocampal interneurons. Network: Comput. Neural Syst. 11: 1–23.

Wang X-J, Buzsáki G (1996) Gamma oscillation by synaptic inhibition in a hippocampal interneuronal network model. J. Neurosci., 16: 6402–6413.

White, JA, Chow CC, Ritt J, Soto-Treviño C, Kopell N (1998) Synchronization and oscillatory dynamics in heterogeneous, mutually inhibited neurons. J. Comput. Neurosci. 5: 5–16.

Wu C, Luk WP, Gillis J, Skinner FK, Zhang L (2004) Size does matter: Generation of intrinsic network rhythms in thick mouse hippocampal slices. J. Neurophysiol. (in press).